Influences of Acid Catalysts on The Microstructure, Bioactivity and Cytotoxicity of Bioactive Glass Nanoparticles Prepared by Spray Pyrolysis

Chao-Kuang Kuo
National Taiwan University of Science and Technology
Liu-Gu Chen
National Tsing Hua University
Chun-Fu Tseng
National Taiwan University of Science and Technology
Yu-Jen Chou (yu-jen.chou@mail.ntust.edu.tw)
National Taiwan University of Science and Technology

Research Article

Keywords: Bioactive glass, Spray pyrolysis, Acid catalysts, Cell viability

Posted Date: September 8th, 2020

DOI: https://doi.org/10.21203/rs.3.rs-69982/v1

Version of Record: A version of this preprint was published at Journal of Non-Crystalline Solids on May 1st, 2021. See the published version at https://doi.org/10.1016/j.jnoncrysol.2021.120710.

Abstract

Bioactive glasses have received considerable attention in the fields of medical and material science and have been applied in applications such as bone implants, tooth fillings, and drug carriers due to their high bioactivity, biocompatibility and biodegradability. Numerous studies applying either conventional glass processes or the sol-gel method have employed Hench's protocol for the fabrication of bioactive glass. However, the effects of various acid catalysts when using spray pyrolysis to synthesize bioactive glass remain unclear. Therefore, in this study, we synthesized bioactive glass nanoparticles using spray pyrolysis and then treated them with the acid catalysts hydrochloric acid, lactic acid and acetic acid. By characterizing the phase information and morphologies of the bioactive glass particles and examining their bioactivity and cytotoxicity, we found that the bioactive glass treated with hydrochloric acid yielded greater cell viability than the lactic acid- and acetic acid-treated specimens; the corresponding mechanisms are discussed in this paper.

Introduction

The introduction of bioactive glass (BG) by Hench et al. in 1969 was a great advance in the field of tissue engineering [1]. Throughout the years, studies have demonstrated its beneficial properties, such as its bioactivity, biocompatibility and biodegradability [2, 3], and it has received considerable attention for various bone and dental applications [4–6]. The surface morphology of BGs plays an important role in determining their bioactivity and cellular properties. To achieve high injectability and beneficial flow properties for specific applications, such as extrusion syringes or injectable cements, particles with spherical shapes are highly desirable [7]. Researchers have reported that in contrast to particles with irregular shapes, spherical particles are able to promote tissue regeneration and minimize inflammation [8, 9]. Therefore, the development of spherical particles is needed.

For the synthesis of BGs, the sol-gel method is the most commonly used process due to its accessibility and versatility, and numerous approaches employing this method have been developed to produce spherical BG particles [10]. For example, Lei et al. reported that the addition of polyethylene glycol (PEG) to the sol-gel method can prompt the formation of BG microspheres [11], and Lukowiak et al. demonstrated the use of a microemulsion to facilitate the production of spherical sol-gel-derived BG [12]. However, the batch procedure of the sol-gel method makes the method difficult to employ at the mass-production scale, and the post heat treatment component of this method can easily lead to phase separation during the calcination stage. In contrast, the spray pyrolysis technique offers the advantages of a continuous procedure and rapid calcination, which allow the products to be rapidly fabricated while minimizing the probability of second phase formation [13].

During the preparation of BGs, acids such as hydrochloric acid, phytic acid and nitric acid are used as catalysts for the hydrolysis of the silicon alkoxide and phosphorous alkoxide to obtain a stable and homogeneous precursor solution [14, 15]. The acid catalysts tend to change the surface morphology of the particles. Studies have reported that acid catalysts with hydroxyl-carboxyl functional groups (i.e.,

acetic acid, citric acid and lactic acid) are important for constructing nanostructures that rely on the interactions of hydrogen bonds with the inorganic precursors [16–18]. Furthermore, the microstructure directly influences the bioactivity of and cellular responses to the specimen. For example, Chen et al. reported that the addition of lactic acid catalyst tends to increase the roughness of nanoscale surface morphologies, which can enhance the bioactivity of the as-prepared particles in vitro [18]. Furthermore, Hong et al. demonstrated that by replacing the conventional polymer pore-forming agent with acetic acid, porous BG particles can be formed with improved bioactivity [19]. In brief, acid catalysts have been proven capable of changing the morphology and increasing the bioactivity of BGs.

Although the effects of acid catalysts on sol-gel derived BG have been studied [20], their effects on spray-pyrolyzed BG, which is formed via a different mechanism, remain unclear. Therefore, in this study, various acids (hydrochloric acid, lactic acid and acetic acid) were employed as the catalysts, and various acid-treated BG specimens were prepared using spray pyrolysis. The phase compositions were characterized using X-ray diffraction (XRD), the surface morphologies were observed using scanning electron microscopy (SEM), and the chemical compositions were determined by energy-dispersive X-ray spectroscopy (EDS). In addition, the bioactivity and cytotoxicity of the BG specimens were examined employing Kukobo's in vitro bioactive test and 3-(4,5-dimethylthiazol-2-yl)-2,5-diphenylte-trazolium bromide (MTT) assay based on ISO standard 10993-5, respectively.

Materials And Methods

Synthesis

The spray pyrolysis method was employed for the preparation of 58S BG specimens (60 mol% SiO_2, 36 mol% CaO, and 4 mol% P_2O_5). Precursor solutions were prepared by dissolving 37.49 g TEOS (tetraethyl orthosilicate, $Si(OC_2H_5)_4$, 99.9 wt%, Showa, Tokyo, Japan), 25.50 g CN (calcium nitrate tetrahydrate, $Ca(NO_3)_2.4H_2O$, 98.5 wt%, Showa, Tokyo, Japan), and 4.37 g TEP (triethyl phosphate, $(C_2H_5)_3PO_4$, 99.0 wt%, Alfa Aesar, Heysham, UK) into 60.00 g ethanol as the sources of Si, Ca and P, respectively. Then, an additional 1.6 g of hydrochloric acid (HCl), lactic acid ($CH_3CH(OH)COOH$) or acetic acid (CH_3COOH) was mixed into each solution independently and stirred at room temperature for 2 h to ensure homogeneity. For the spray pyrolysis process, each precursor solution was poured into an ultrasonic atomizer (KT-100A, King Ultrasonic, New Taipei, Taiwan) that operates under a frequency of 1.65 MHz. Droplets were atomized and diverted into a tubular furnace (D-80, Dengyng, New Taipei, Taiwan) with three heating zones set at 250, 550 and 350°C. The resulting BG specimens were collected at the end of the furnace by an earthed electrostatic stainless steel collector applied with high voltage of 16 kV. The HCl-treated, lactic acid-treated and acetic acid-treated BG specimens were denoted HBG, LBG and ABG, respectively.

Characterization

The phase compositions of the HBG, LBG and ABG specimens were examined using an XRD (D2 Phaser, Bruker, Karlsruhe, Germany) with Ni-filtered Cu-Kα radiation. The XRD patterns were recorded with

diffraction angles ranging from 20° to 80°, and the scanning rate was set at 6° per minute. Next, the surface morphologies were obtained by field emission SEM (JSM-6500F, JEOL, Tokyo, Japan). The SEM samples were prepared by dispensing the powders onto SEM holders with conductive carbon tapes while images were taken at 15 kV to ensure sufficient contrast. In addition, the chemical compositions were analyzed using EDS (X-Max 50 mm^2, Oxford Instruments, High Wycombe, UK), and the particle size distributions were computed from several SEM images and more than 300 particles.

For the evaluation of bioactivity, simulated body fluid (SBF), which has a similar ionic concentration as human plasma, was used according to Kokubo's protocol [21]. By immersing BG specimens into SBF, test specimens were prepared with a solid to liquid ratio of 1 mg to 5 mL. The pH of the solutions were maintained at 7.4, and all of solutions were placed in a thermostatic orbital shaker and stirred at 37°C for 24 h. The resulting powders were washed with deionized water and acetone three times and then dried in an oven at 70°C for 24 h. Finally, both XRD and SEM were employed to analyze the bioactivity of each specimen.

Assessment of cell viability was carried out by 3-(4,5-dimethylthiazol-2-yl)-2,5-diphenylte-trazolium bromide (MTT) assay. The viabilities of all BG specimens were determined using serial dilutions of the samples according to the standard testing protocol ISO 10993-5. Initially, all specimens were sterilized using an autoclave and dispersed in minimum essential medium (MEM) at one of several extraction concentrations: 20%, 40%, 60%, 80% and 100%. The seeded cells were cultured at a density of $2 \cdot 10^4$ cells/cm^3 with BG specimens on a 24-well plate and then incubated at 37°C for 24 h in a humidified atmosphere of 95% air and 5% CO_2. Next, the media were removed, 300 µL MTT reagent was added to each well, and the plates were incubated in a CO_2 incubator at 37°C for 72 h. Finally, the medium was aspirated, and 200 µL of dimethyl sulfoxide (DMSO) was added to each well. The solution was then transferred to a 96-well plate, and the optical density was measured at a wavelength of 570 nm using a microplate reader (Multiskan Go, Thermo Scientific, USA).

Results

Figure 1 shows the XRD patterns of the spray-pyrolyzed HBG, LBG and ABG specimens. For the HBG specimen, no distinct diffraction peaks were observed, with only broad bands appearing between 20° to 40°, suggesting that the structure of the specimen was amorphous. The LBG and ABG specimens exhibited XRD patterns similar to that of the HBG specimen, indicating that all BG specimens were successfully synthesized with glassy phases using spray pyrolysis.

SEM images of all BG specimens are shown in Fig. 2 and demonstrate that all BG particles exhibited a spherical shape, with diameters ranging from 0.5 to 3 µm. As shown in Fig. 2 (a), the HBG specimen exhibited only one surface morphology, smooth sphere. Unlike the HBG specimen, the LBG specimen exhibited two morphologies, smooth sphere and rough sphere, as shown in Fig. 2 (b). Furthermore, in addition to exhibiting smooth and rough sphere morphologies, the ABG specimen exhibited an additional

surface morphology, porous sphere. The three surface morphologies of smooth, rough and porous spheres of the BG specimens were denoted as Type I, II and III, respectively.

Based on the SEM images, particle size distributions were determined, as shown in Fig. 3. The average particle sizes were 1.05 ± 0.48, 1.14 ± 0.47 and 1.14 ± 0.48 μm for the HBG, LBG and ABG specimens, respectively. Approximately 80% of the particles ranged in size between 0.5 to 1.5 μm; no significant differences in particle size were found among the specimens. The particle morphology distributions are shown in Fig. 4. As shown in the figure, the HBG specimen had a single morphology, smooth sphere (100% Type I). In contrast to the HBG specimen, the LBG specimen exhibited two morphologies, with relative percentages of 52.8% and 47.2% for Type I and Type II particles, respectively. For the ABG specimen, three types of morphology were observed; the relative percentages of Type I, II and III particles were 19.6%, 29.4% and 51.0%, respectively.

Table 1 shows the chemical compositions of the BG specimens determined from the EDS spectra. The percentages of Si, Ca and P were 55.16 ± 0.37, 35.27 ± 1.35 and 9.56 ± 0.98%, respectively, for the HBG specimen; 54.45 ± 1.21, 36.20 ± 0.45, and 9.35 ± 0.89, respectively, for the LBG specimen; and 53.93 ± 0.65, 36.40 ± 0.52, and 9.71 ± 0.18, respectively, for the ABG specimen. These results show that all acid-treated BG specimens were successfully synthesized with the nominal precursor composition, indicating that the acid treatments did not affect the chemical composition of the BG specimens.

Table 1
Atomic compositions of spray-pyrolyzed HBG, LBG and ABG specimens

Specimen	Si	Ca	P
HBG	55.16 ± 0.37	35.27 ± 1.35	9.56 ± 0.98
LBG	54.45 ± 1.21	36.20 ± 0.45	9.35 ± 0.89
ABG	53.93 ± 0.65	36.40 ± 0.52	9.71 ± 0.18
			Unit: atomic%

SEM images of all BG specimens after the in vitro bioactivity test are shown in Fig. 5. Comparison of these images to the SEM images of as-prepared specimens shown in Fig. 2 revealed that the surface morphologies of all BG specimens changed, with a layer of needle-shaped HA having formed on the surface of each particle. However, it is difficult to quantify the bioactivity of each BG specimens from the SEM images. Figure 6 shows the XRD patterns of the HBG, LBG and ABG specimens after immersion in SBF for 24 h. All BG specimens showed diffraction peaks of (002) and (211) at 25.8° and 31.7°, in contrast to the amorphous structure as shown in Fig. 1, indicating the formation of HA (JCPDS No. 89-6495). To determine the bioactivity, background subtraction was performed, and peak area analysis was conducted to quantify the crystallinity of each specimen. The results show that the peak area of the (211) plane was 384, 388 and 392 a.u. for the HBG, LBG and ABG specimens, respectively.

Evaluations of cytotoxicity of the HBG, LBG, and ABG specimens were carried out by MTT assay, and the results are shown in Fig. 7. Cell viability was measured as the percentage of living cells for each of the different extract concentrations. As shown in the figure, all BG specimens passed the standard cell viability level of 70% at extraction concentrations of 20%, 40%, 60% and 80%, indicating that all specimens were nontoxic when applied at extraction concentrations lower than 80%. However, at the extraction concentration of 100%, the cell viability for HBG, LBG and ABG specimens decreased to approximately 78%, 61% and 51%, respectively. Only the HBG specimen passed the standard cell viability level at the extraction concentration of 100%.

Discussion

Based on the XRD patterns shown in Fig. 1, the crystallographic structures of the BG specimens treated with the various acid catalysts were all recognized as amorphous. In addition, chemical compositions determined from the EDS spectra (Table 1) indicated that all the acid-treated BG specimens were synthesized with the nominal precursor composition of 58S. These results demonstrate the successful synthesis of the BG specimens and show that the treatments of the acid catalysts affected neither the chemical composition nor the phase composition of the spray-pyrolyzed BG specimens.

Based on the SEM images shown in Fig. 2, the morphologies of the BG specimens are discussed in the following. The micrographs show that the particle diameters of all BG specimens ranged from 0.5 to 3 μm. Owing to the lack of nanoparticles with diameters less than 100 nm, the formation mechanism of all BG particles in the spray pyrolysis technique can be categorized as the typical “one-particle-per-droplet” formation instead of “gas-to-particle” conversion [22]. In addition, with regard to the surface morphology, three types were observed, smooth, rough and porous, in contrast to the surface morphology of sol-gel derived BG specimens [20]. The Type I morphology, smooth sphere, was observed in all BG specimens. The formation of Type I particles can be categorized as the typical spray pyrolysis mechanism of “volume precipitation” [22], where all precursors precipitate simultaneously during the calcination stage and result in the morphology of a smooth sphere. The Type II morphology, rough sphere, was found in both the LBG and ABG specimens. For the LBG specimen, it is believed that with the addition of the lactic acid, hydroxyl–carboxylic bonding interactions with the inorganic precursor occurred [18], resulting in a rough surface morphology after the removal of the lactic acid molecules. In contrast, for the ABG specimen, the added acetic acid interacted with TEOS in the precursor solution to form ethyl acetate [19, 23]. The product then aggregated on the surface, resulted in the rough-sphere morphology after the calcination stage. The Type III morphology, porous sphere, was observed only in the ABG specimen. The porous particles formed owing to the release of CO_2 and H_2O during the decomposition of acetic acid [24]. In brief, unlike sol-gel-derived BG specimens, all of the spray-pyrolyzed BG specimens in this study exhibited a consistent spherical morphology. When the particles were treated with the various acid catalysts, changes in microstructure occurred according to the mechanisms described above.

Below, we discuss the bioactivity and cell viability of all of the BG specimens. In the XRD patterns shown in Fig. 6, a higher peak area represents a higher HA crystallinity; thus, the order of bioactivity can be derived as ABG > LBG > HBG. This ordering reflects the increase in surface area contributed by the rough and porous particles (Type II and Type III), as demonstrated in various reports [25, 26]. Regarding cell viability, studies have demonstrated that a smooth particle surface has a positive effect on cell viability by allowing cells to spread evenly over the surface [27, 28]. Type I particles accounted for 100%, 52.8% and 19.6% of the particle populations of the HBG, LBG and ABG specimens, respectively, and the cytotoxicity tests showed that the cell viability associated with the HBG, LBG and ABG specimens was 78%, 61% and 51%, respectively, indicating a positive effect of Type 1 morphology on cell viability. In summary, in this study, we demonstrated that among all of the studied acid-treated specimens, the HCl-treated BG specimen was the most bioactive and cytocompatible.

Conclusions

In this study, spray-pyrolyzed BG specimens treated with various acid catalysts were successfully synthesized. The morphological characterization revealed that the HBG specimen exhibited the typical spray-pyrolysis morphology of smooth spheres, whereas the LBG and HBG specimens exhibited the additional morphologies of rough and porous spheres. The corresponding formation mechanisms were considered, and the in vitro bioactive tests suggested that all specimens were bioactive. Furthermore, the cytotoxicity tests demonstrated that the HBG specimen was associated with greater cell viability than LBG and ABG specimens owing to the favorable effects of smooth surfaces on cell proliferation. To conclude, the results show that the type of acid catalyst plays an important role in determining the morphology, bioactivity and cytotoxicity of spray-pyrolyzed BG particles and that HCl-treated BG has potential for facilitating bone growth and promoting cell proliferation.

Declarations

Acknowledgments

The authors acknowledge the financial support from Ministry of Science and Technology of Taiwan (grant number MOST 108-2218-E-011-035).

References

1. Hench LL, Splinter RJ, Allen WC, Greenlee TK (1971) Bonding mechanisms at the interface of ceramic prosthetic materials. J Biomed Mater Res 5:117–141
2. Hench LL (1991) Bioceramics: From concept to clinic. J Am Ceram Soc 74:1487–1510
3. Cao W, Hench LL (1996) Bioactive materials. Ceram Int 22:493–507
4. Chatzistavrou X, Tsigkou O, Amin HD, Paraskevopoulos KM, Salih V, Boccaccini AR (2012) Sol–gel based fabrication and characterization of new bioactive glass–ceramic composites for dental applications. J Eur Ceram Soc 32:3051–3061

5. Vallet-Regí M, Ceramics for medical applications, J. Chem. Soc. Dalton, (2001) 97–108
6. Xia W, Chang J (2006) Well-ordered mesoporous bioactive glasses (mbg): A promising bioactive drug delivery system. J Control Release 110:522–530
7. Kretlow JD, Klouda L, Mikos AG (2007) Injectable matrices and scaffolds for drug delivery in tissue engineering. Adv Drug Deliver Rev 59:263–273
8. Paul W, Sharma CP (1999) Development of porous spherical hydroxyapatite granules: Application towards protein delivery. J Mater Sci: Mater Med 10:383–388
9. Manzano M, Aina V, Areán CO, Balas F, Cauda V, Colilla M, Delgado MR (2008) M. Vallet-Regí, Studies on mcm-41 mesoporous silica for drug delivery: Effect of particle morphology and amine functionalization. Chem Eng J 137:30–37
10. Zheng K, Boccaccini AR (2017) Sol-gel processing of bioactive glass nanoparticles: A review. Adv Colloid Interfac 249:363–373
11. Lei B, Chen X, Wang Y, Zhao N (2009) Synthesis and in vitro bioactivity of novel mesoporous hollow bioactive glass microspheres. Mater Lett 63:1719–1721
12. Lukowiak A, Lao J, Lacroix J, Nedelec J-M (2013) Bioactive glass nanoparticles obtained through sol–gel chemistry. Chem Commun 49:6620–6622
13. Shih S-J, Chou Y-J, Chien I-C (2012) One-step synthesis of bioactive glass by spray pyrolysis. J Nanopart Res 14:1–8
14. Meiszterics A, Havancsák K, Sinkó K (2013) Catalysis, nanostructure and macroscopic property triangle in bioactive calcium-containing ceramic systems. Mater Sci Eng C 33:1371–1379
15. Li A, Qiu D (2011) Phytic acid derived bioactive Cao–P_2O_5–SiO_2 gel-glasses. J Mater Sci: Mater Med 22:2685–2691
16. Shah AT, Ain Q, Chaudhry AA, Ahmad S, Zarif F, Siddiqi SA, Qasim Sb, Görke O, Khan AS (2018) I.u. Rehman, Acid catalysed synthesis of bioactive glass by evaporation induced self assembly method. J Non-Cryst Solids 479:1–8
17. Lei B, Chen X, Wang Y, Zhao N, Du C, Fang L (2010) Surface nanoscale patterning of bioactive glass to support cellular growth and differentiation. J Biomed Mater Res A 94A:1091–1099
18. Chen X, Lei B, Wang Y, Zhao N (2009) Morphological control and in vitro bioactivity of nanoscale bioactive glasses. J Non-Cryst Solids 355:791–796
19. Hong B-J, Hsiao C-W, Bakare FF, Sun J-T, Shih S-J (2018) Effect of acetic acid concentration on pore structure for mesoporous bioactive glass during spray pyrolysis. Materials 11:963
20. Lei B, Chen X, Koh Y-H (2011) Effects of acidic catalysts on the microstructure and biological property of sol–gel bioactive glass microspheres. J Sol-gel Sci Techn 58:656–663
21. Kokubo T, Kushitani H, Ohtsuki C, Sakka S, Yamamuro T (1992) Chemical reaction of bioactive glass and glass-ceramics with a simulated body fluid. J Mater Sci: Mater Med 3:79–83
22. Messing GL, Zhang S-C, Jayanthi GV (1993) Ceramic powder synthesis by spray pyrolysis. J Am Ceram Soc 76:2707–2726

23. Arenas LT, Simm CW, Gushikem Y, Dias SLP, Moro CC, Costa TMH, Benvenutti EV (2007) Synthesis of silica xerogels with high surface area using acetic acid as catalyst. J Brazil Chem Soc 18:886–890
24. Schoofs GR, Benziger JB (1984) Decomposition of acetic acid monomer, acetic acid dimer, and acetic anhydride on ni(111), Surf. Sci 143:359–368
25. Bakare FF, Chou Y-J, Huang Y-H, Tesfay AH, Moriga T, Shih S-J (2019) Correlation of morphology and in-vitro degradation behavior of spray pyrolyzed bioactive glasses. Materials 12:3703
26. Yan X, Yu C, Zhou X, Tang J, Zhao D (2004) Highly ordered mesoporous bioactive glasses with superior in vitro bone-forming bioactivities. Angew Chem Int Edit 43:5980–5984
27. Barrioni BR, Naruphontjirakul P, Norris E, Li S, Kelly NL, Hanna JV, Stevens MM, Jones JR, Pereira MdM (2019) Effects of manganese incorporation on the morphology, structure and cytotoxicity of spherical bioactive glass nanoparticles. J Colloid Interf Sci 547:382–392
28. A.A.R. de Oliveira AAR, de Souza DA, Dias LLS, de Carvalho SM, HS Mansur, M. de (2013) Magalhães Pereira, Synthesis, characterization and cytocompatibility of spherical bioactive glass nanoparticles for potential hard tissue engineering applications. Biomed Mater 8:025011

Figures

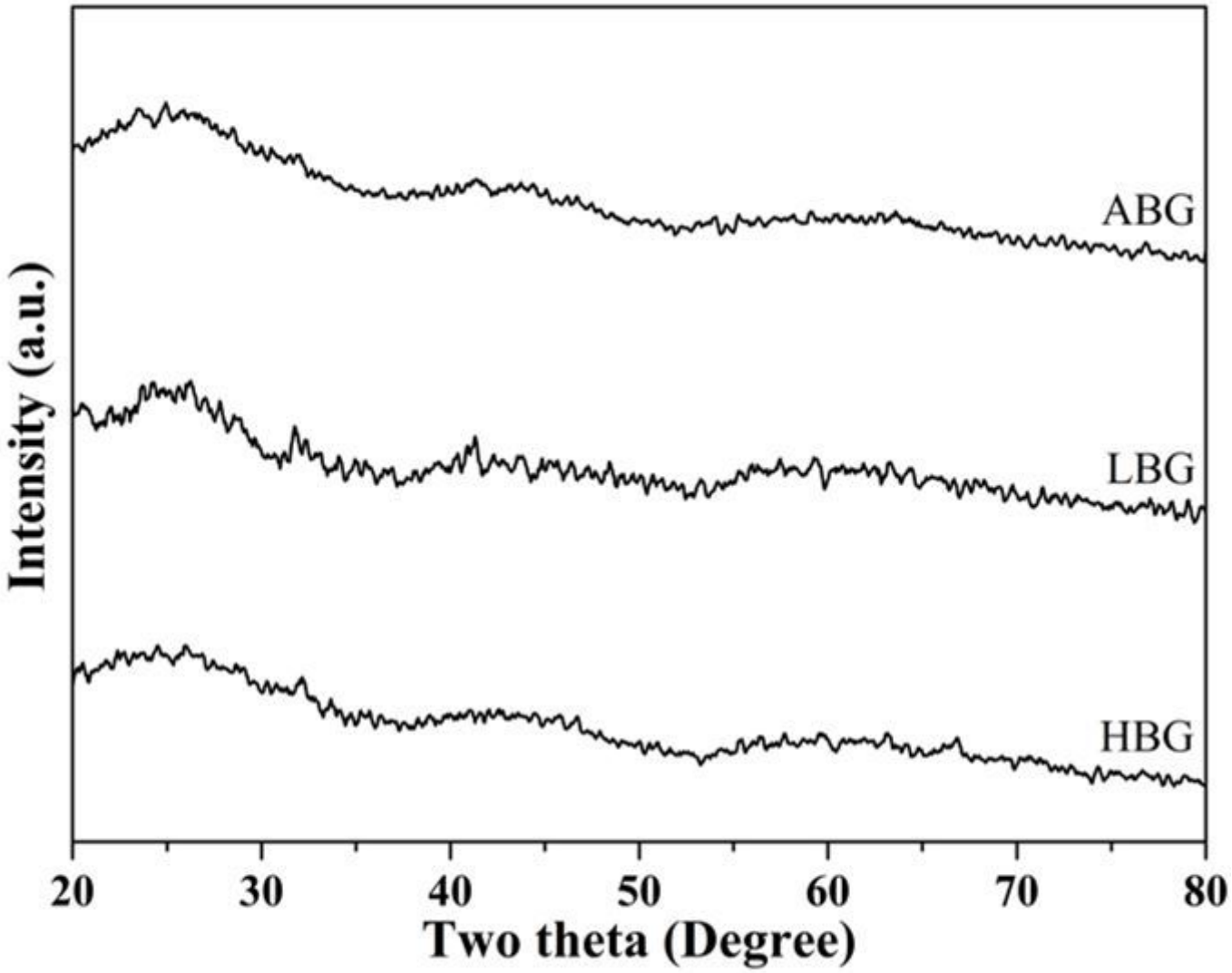

Figure 1

XRD patterns of spray-pyrolyzed BG specimens treated with hydrochloric acid, lactic acid and acetic acid (denoted HBG, LBG and ABG).

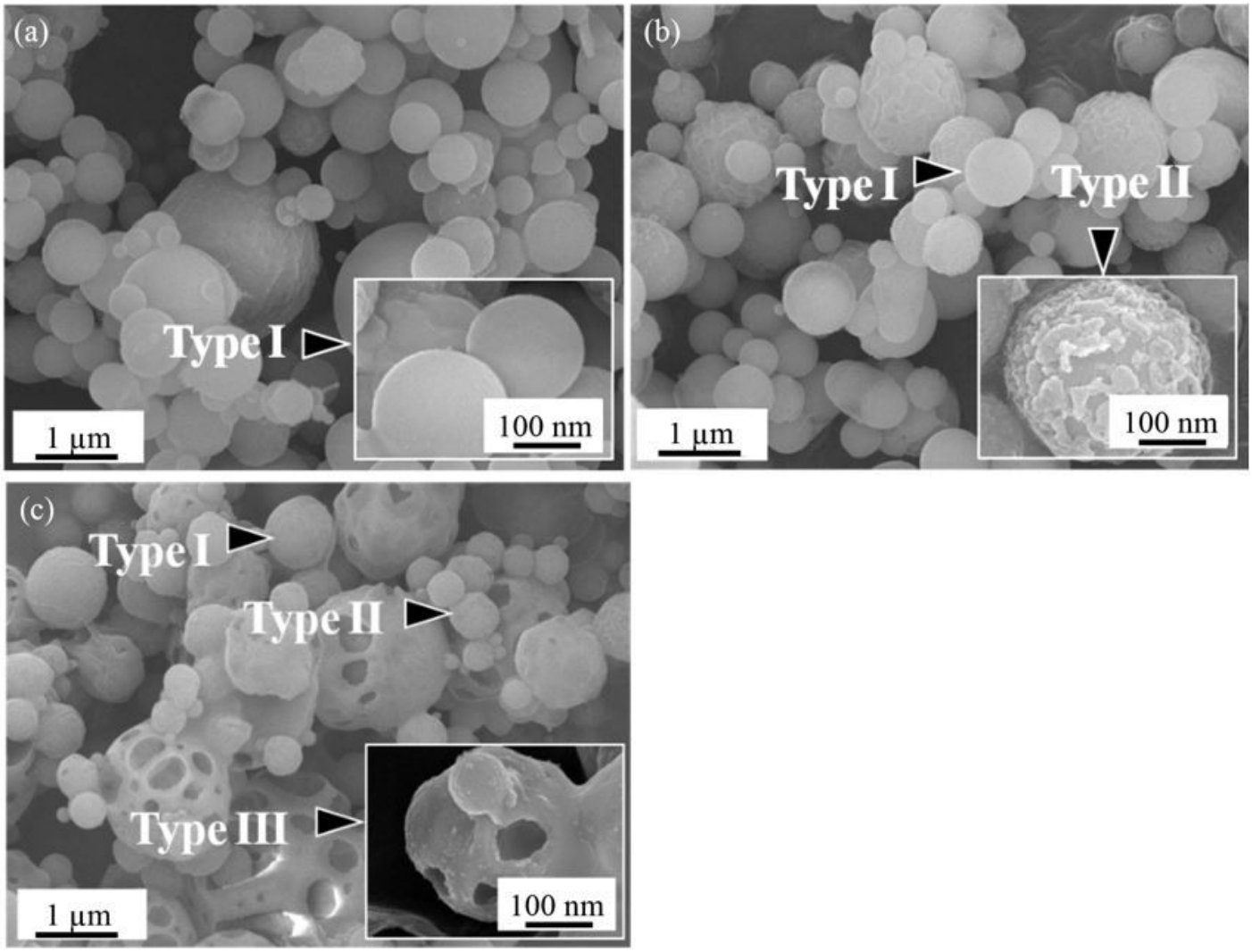

Figure 2

SEM images of spray-pyrolyzed (a) HBG, (b) LBG and (c) ABG specimens. The black arrows of Type I, II and III particles represent the three surface morphologies of smooth, rough and porous.

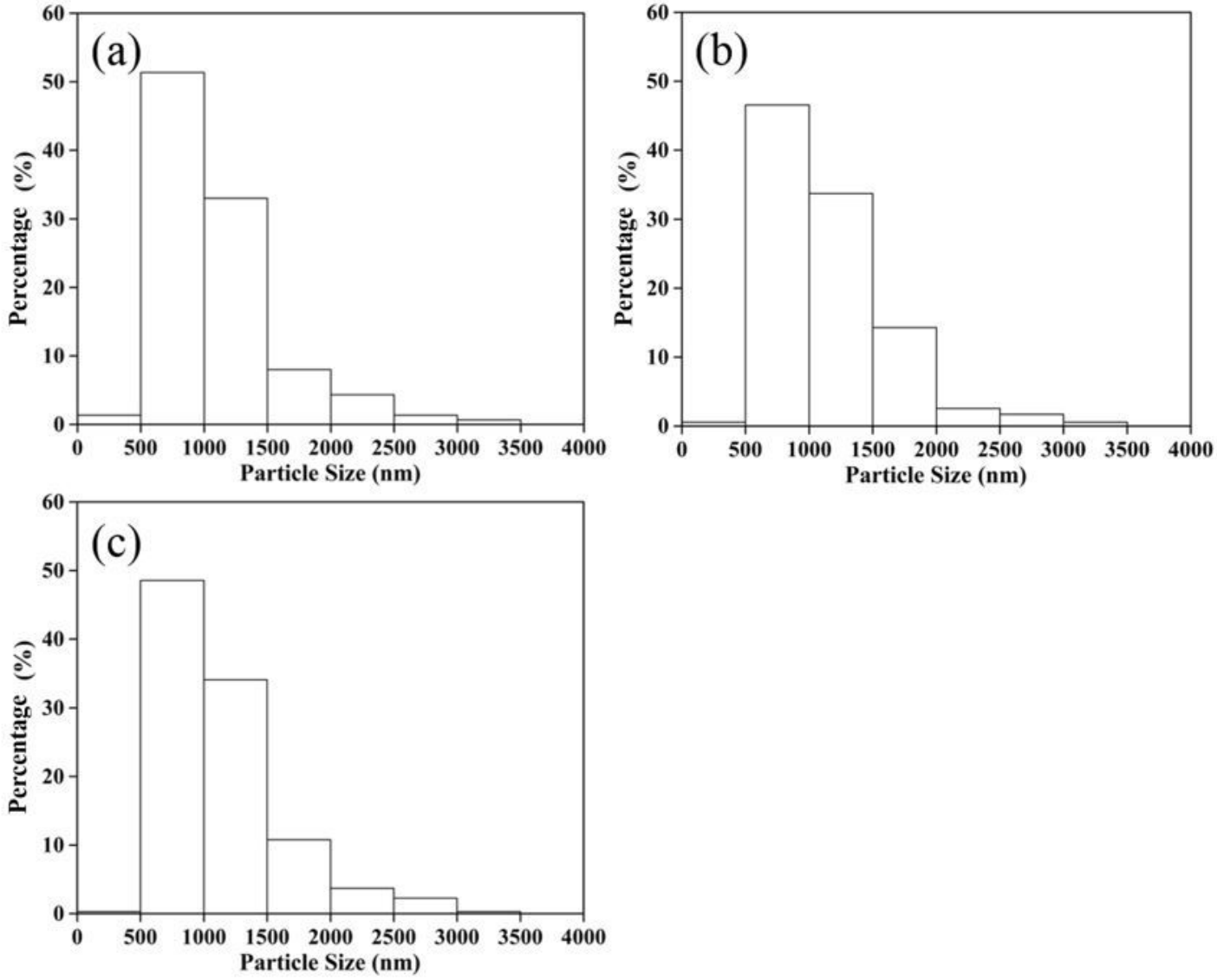

Figure 3

Particle size distributions of spray-pyrolyzed (a) HBG, (b) LBG and (c) ABG specimens.

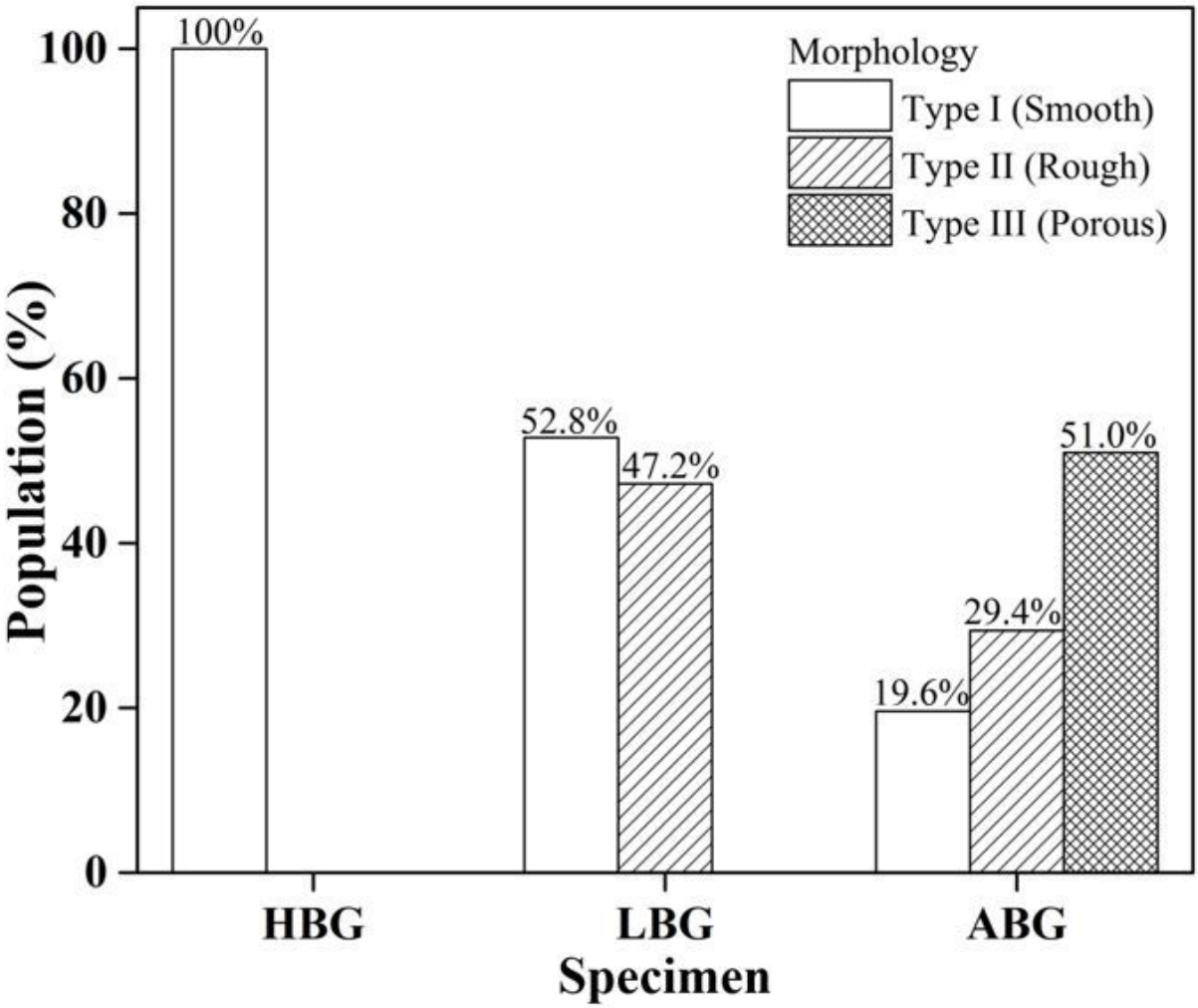

Figure 4

Relative fractions of spray-pyrolyzed HBG, LBG and ABG particles with the morphological types of smooth, rough and porous.

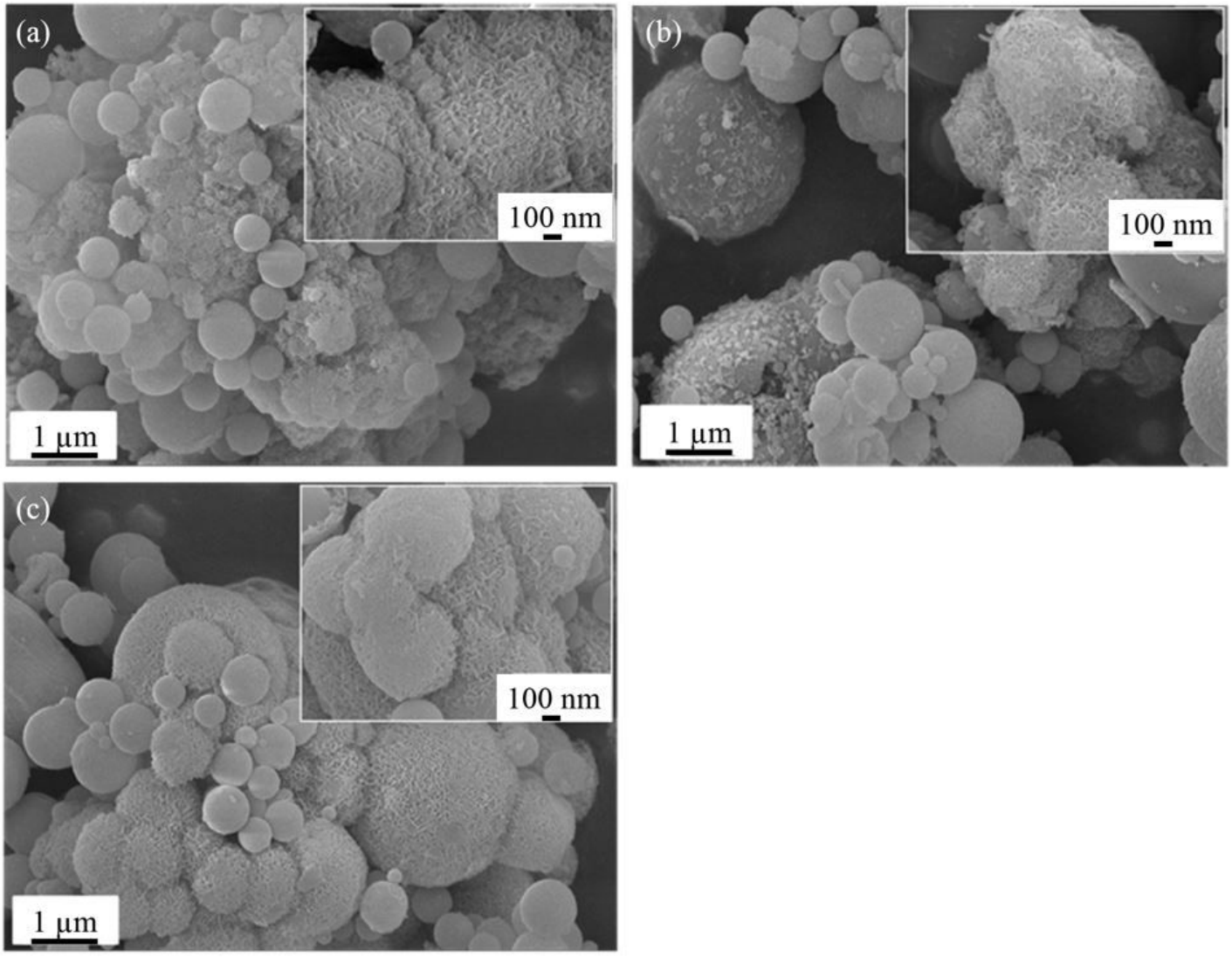

Figure 5

SEM images of spray-pyrolyzed (a) HBG, (b) LBG and (c) ABG specimens after immersion in SBF for 24 h.

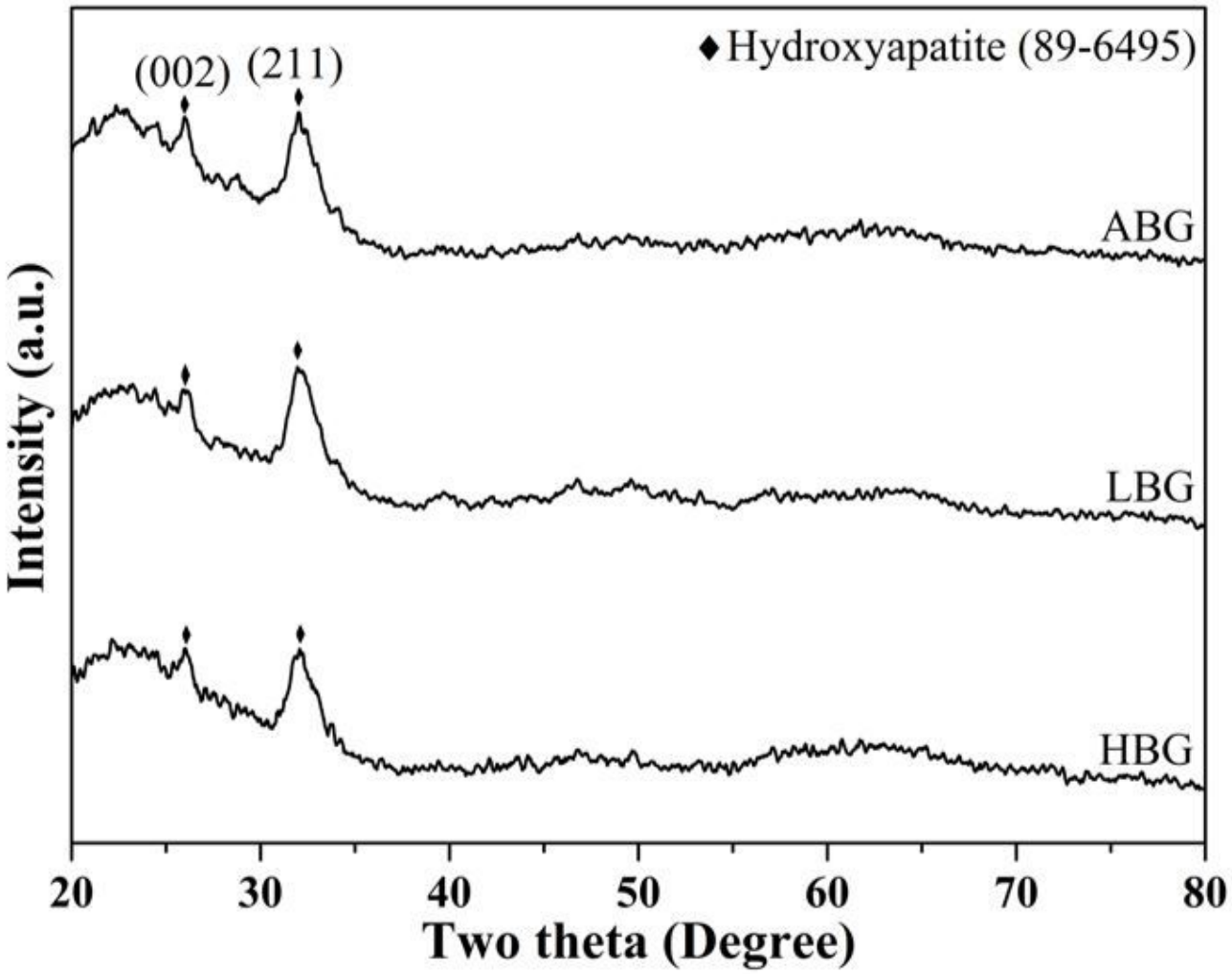

Figure 6

XRD patterns of spray-pyrolyzed HBG, LBG and ABG specimens after immersion in SBF for 24 h.

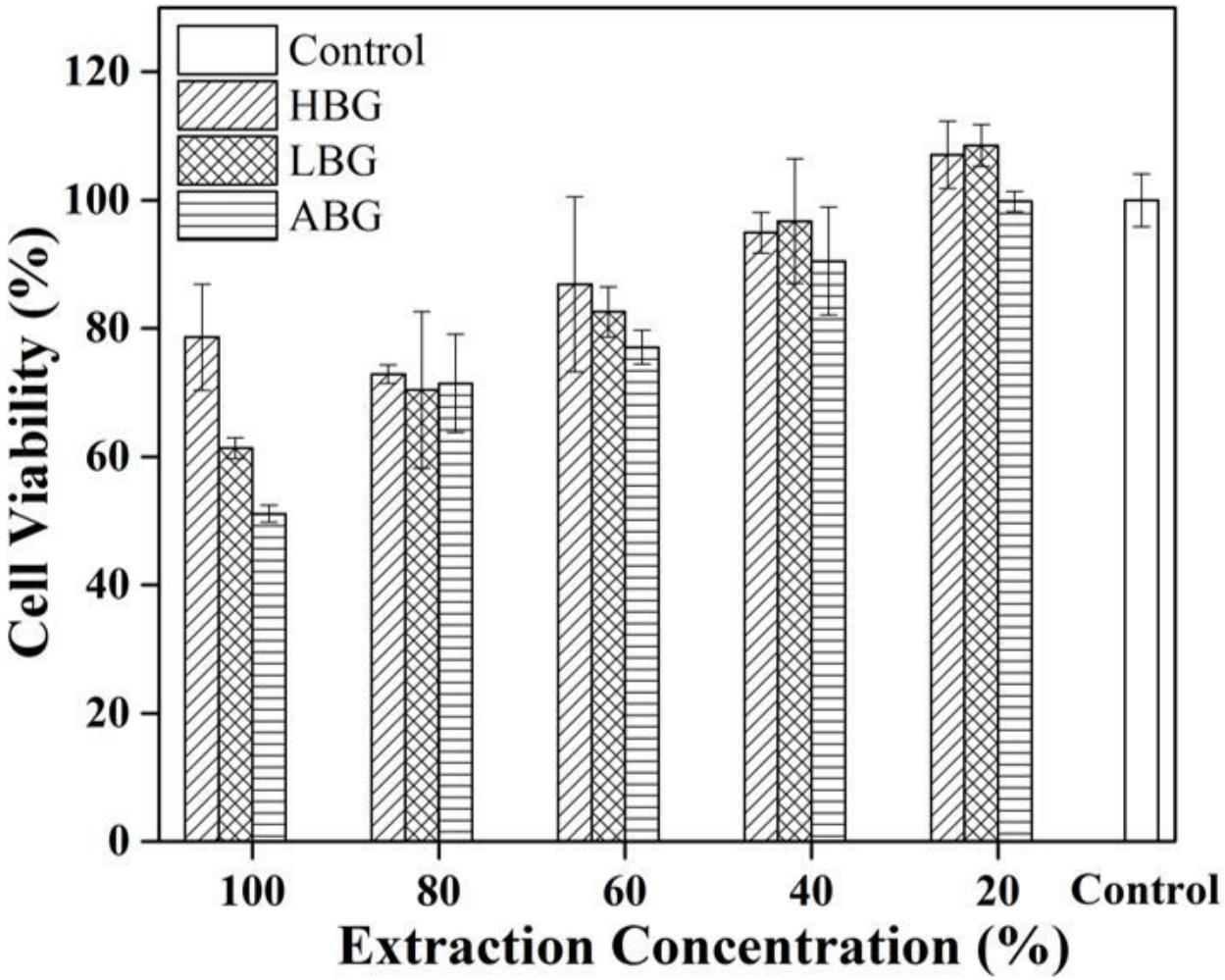

Figure 7

Cell viability associated with spray-pyrolyzed HBG, LBG and ABG specimens as a function of extract concentration.